Journal of
Applied Crystallography
ISSN 0021-8898

Received 22 February 2010
Accepted 9 June 2010

The extended *Q*-range small-angle neutron scattering diffractometer at the SNS

J. K. Zhao,* C. Y. Gao and D. Liu

Neutron Scattering Sciences Division, Oak Ridge National Laboratory, Oak Ridge, TN 37831, USA. Correspondence e-mail: zhaoj@ornl.gov

The extended *Q*-range small-angle neutron scattering diffractometer (EQ-SANS) at the Spallation Neutron Source (SNS), Oak Ridge, is designed for wide neutron momentum transfer (Q) coverage, high neutron beam intensity and good wavelength resolution. In addition, the design and construction of the instrument aim to achieve a maximum signal-to-noise ratio by minimizing the background. The instrument is located on the high-power target station at the SNS. One of the key components in the primary flight path is the neutron optics, consisting of a curved multichannel beam bender and sections of straight neutron guides. They are optimized to minimize neutron transport loss, thereby maximizing the available flux on the sample. They also enable the avoidance of a direct line of sight to the neutron moderator at downstream locations. The instrument has three bandwidth-limiting choppers. They allow a novel frame-skipping operation, which enables the EQ-SANS diffractometer to achieve a dynamic Q range equivalent to that of a similar machine on a 20 Hz source. The two-dimensional low-angle detector, based on ^{3}He tube technologies, offers very high counting rates and counting efficiency. Initial operations have shown that the instrument has achieved its design goals.

1. Introduction

High-flux steady-state research reactors have been the traditional home of state-of-the-art small-angle neutron scattering (SANS) diffractometers (Ibel, 1976; Koehler, 1986; Glinka *et al.*, 1998). New generations of pulsed spallation sources have created significant challenges for the design of high-performance SANS instruments. The performance of SANS diffractometers is often limited by the neutron flux and the experimental background. In both these areas, reactor sources are well suited for SANS instruments: extremely bright cold neutron sources at leading research reactors offer very high time-averaged neutron flux, and SANS instruments on reactors are typically built in an extended guide hall, where background is reduced to a minimum. In comparison, the current generation of pulsed sources still lags behind in time-averaged flux. However, the time structure of a pulsed source allows neutron scattering instruments to operate in the time-of-flight (TOF) mode and use wider neutron bandwidth, thereby increasing the dynamic range in neutron momentum transfer Q [$Q = (4\pi/\lambda)\sin\theta$, where θ is half the scattering angle and λ the wavelength of the incident radiation] (Ishikawa *et al.*, 1986; Crawford & Carpenter, 1988; Crawford *et al.*, 1989; Seeger & Hjelm, 1991; Heenan *et al.*, 1997; Serdyuk, 1995). In fact, some of the new SANS instruments at steady-state sources are designed to take advantage of TOF operations by using pulse-generating choppers (Dewhurst, 2008). The wavelength resolution of a spallation-based pulsed source is typically much better than that of a velocity selector, which is commonly used as the monochromator on reactor-based SANS instruments. In addition, scattering data from TOF SANS are time-tagged, making the study of time-dependent phenomena readily accessible.

The short-pulse high-power target station of the Spallation Neutron Source (SNS) at the Oak Ridge National Laboratory, Tennessee, USA, has a design power of 1.4 MW and operates at a repetition rate of 60 Hz. While the high beam power offers the brightest pulsed neutron beam to date, the 60 Hz repetition rate is not optimal for small-angle neutron scattering instruments. Such a high repetition rate puts a limit on the length of a SANS instrument and its usable neutron bandwidth. This bandwidth is determined by the length of the instrument together with the time width of a frame, *i.e.* the time interval between two consecutive source pulses. It can be readily calculated from the simple time, speed and distance relationship for the traveling neutrons. Since the speed v of a neutron is related to its wavelength λ by $v = h/(m_N\lambda)$, the frame bandwidth $\Delta\lambda$ is therefore given in ångström by $\Delta\lambda = h/(m_N fL) = 3956/(fL)$, where h is Planck's constant, m_N is the mass of a neutron, L is the instrument length, *i.e.* the distance between the detector and the moderator given in meters, and f is the repetition rate of the source. The inverse of f is the frame time width. With $f = 60$ Hz for the SNS, the frame bandwidth is only about 3 Å for a 20 m-long instrument. This falls far short of the usable source spectrum offered by the SNS cold moderator.

The EQ-SANS diffractometer is designed to be a workhorse instrument at the SNS. In this paper, the design, construction and initial operation of the EQ-SANS instrument are presented. The key components of the instrument, including the neutron optics, chopper system and detector, are discussed. In addition, the advantage of operating the instrument in a novel frame-skipping mode is demonstrated. Frame skipping allows this instrument, on the 60 Hz SNS target station, to have a dynamic range that is equivalent to a 20 Hz instrument. Finally, the first scattering data from the instrument are presented.

In the current work, the following conventions are used:

(*a*) The terms target and source, when used in the context of the SNS, refer to the SNS mercury target or the target–moderator assembly.

(*b*) The terms moderator, source and neutron source, when used in the context of the EQ-SANS instrument, refer to the cold neutron moderator that EQ-SANS views.

(*c*) The term source slit refers to the collimator slit upstream from the sample, which is the source in the sense of pinhole SANS (*i.e.* source–sample–detector).

(*d*) Unless otherwise noted, all component locations refer to the surface of the neutron moderator as their coordinate origin.

(*e*) Frame numbers are used loosely. Strictly speaking, frame 1 starts at time zero, *i.e.* at the time when the neutron pulse is generated. Frames 2, 3 *etc.* then follow. However, if a neutron band as selected by the bandwidth choppers does not line up with the frame boundaries as defined by the source pulses, such as the example discussed in §4.3, we shall call it frame 1 if neutrons from its leading edge arrive at the detector before the occurrence of the next source pulse, and so on.

2. Instrument geometry

The extended Q-range small-angle neutron scattering diffractometer EQ-SANS is located on Beamline 6 at the SNS. It has pinhole geometry and views the top-downstream coupled supercritical hydrogen moderator (Iverson *et al.*, 2002). In an optimal pinhole SANS geometry, the upstream collimation slit, or the source slit, and the detector should be located at equal distances from the sample. The longer these distances are, the lower the accessible Q values the machine will have. For maximized flux on the sample, the source should be twice as large as the sample, which then requires a beam stop on the detector that is at least four times the size of the sample. In this geometry, the total length of the instrument has to be long enough to accommodate adequate collimation spaces and sample-to-detector distances (SDDs). On the other hand, longer instruments on pulsed sources mean that the usable frame bandwidth becomes narrower. The optimal compromise for EQ-SANS is a fixed primary flight path of 14 m and a variable secondary flight path of ∼1–10 m. Fig. 1 shows a schematic representation of the EQ-SANS layout, with the locations of all major components indicated. Fig. 2 shows four selected components of the instrument. The variable total instrument length of 15–24 m corresponds to a

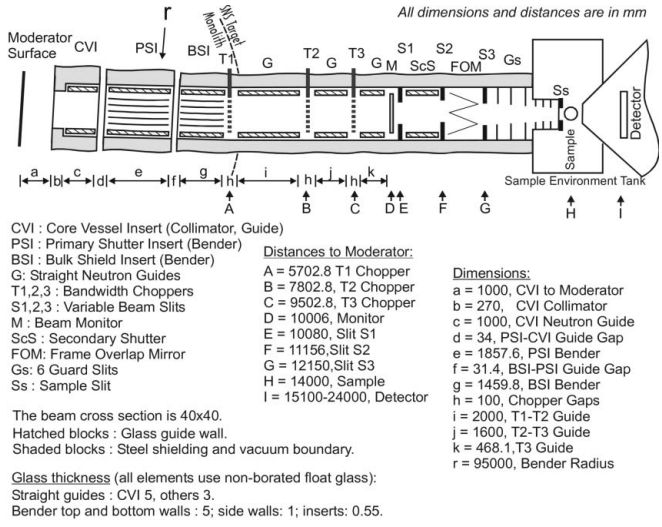

Figure 1
Schematic representation of the extended Q-range small-angle neutron scattering instrument at the SNS. Labels for each component are located directly above that component. The component dimensions (lower-case letters) and locations (capital letters) are marked below.

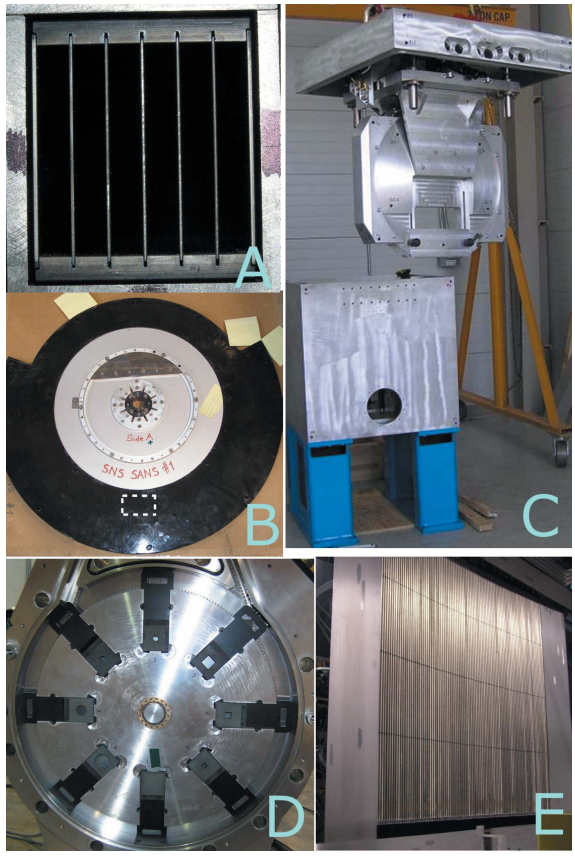

Figure 2
Selected EQ-SANS components. A: Neutron beam bender in the primary beam shutter. B: Bandwidth chopper disc. The dark area is coated with neutron absorber (^{10}B), and the dashed line indicates the cut-out option for a future high-speed upgrade. C: Bandwidth chopper housing with a dummy chopper attached to the lid. The chopper can be translated up and down by 10 cm. D: Slit selections on the collimation slit wheel. E: The low-angle detector array. See text for full details.

frame bandwidth of $\Delta\lambda \simeq 2.7$–4.4 Å at the 60 Hz repetition rate. Beam collimation starts after the beam monitor at 10 m (M, Fig. 1), giving a maximum collimation length of ∼4 m. When the detector is more than 4 m away from the sample (SDD > 4 m), the instrument is obviously no longer in an optimal pinhole geometry and smaller collimation slits will have to be used. In theory, the source slit can be located before the last bandwidth chopper T3 (Fig. 1). In practice, the associated engineering complexities outweigh any gains in such an arrangement. In addition, it is not desirable to have any materials in the beam after the collimation slit, including beam monitors and rotating chopper discs, since such materials would degrade the collimation quality of the neutron beam and create background around the zero scattering angle.

3. Neutron beam optics

The EQ-SANS neutron optics is designed to minimize transport loss for thermal and cold neutrons and to avoid the direct line of sight of the moderator at downstream locations. The optics parameters are largely based on initial instrument design choices (Zhao, 2000*a*,*b*, 2003*a*) with further optimizations under real-life spatial constraints (Fig. 1). The SNS produces up to 1 GeV neutrons at the target at time zero, namely at the time when the 1 GeV proton pulse from the accelerator hits the mercury target. There are generally two options to shield against these fast neutrons. One is to use a T0 chopper located very close to the SNS target monolith, but such a chopper carries considerable operational and maintenance burdens. The other is to use curved neutron optics to transport thermal and cold neutrons but not fast ones. The EQ-SANS diffractometer uses a curved beam bender (Fig. 2A) in combination with straight guides and a collimator. The neutron guides and benders are made of non-borated float glass coated with a supermirror multilayer. Except on the convex sides of the curved bender channels, the supermirror has a critical neutron reflection angle of $3.5\theta_c$, θ_c being the total reflection angle of natural nickel, which is 0.1° Å^{-1}. The convex sides of the bender channel walls have $2\theta_c$ coatings. The guide and bender assembly was manufactured by Swiss-Neutronics Inc. (http://www.swissneutronics.ch). For all the supermirror coatings, the reflectivity is close to 100% when the reflection angle is less than θ_c. It drops to no less than 72% at $3.5\theta_c$ for the $3.5\theta_c$ supermirrors and no less than 90% at $2\theta_c$ for the $2\theta_c$ supermirrors. The initial collimator (not to be confused with the collimating slits for thermal neutrons before the sample) is a 270 mm-long steel piece with a beam opening of 40 × 40 mm (section b, Fig. 1). The 40 × 40 mm beam cross section is chosen based on the fact that, in most small-angle scattering experiments, the samples are no larger than 20 × 20 mm. Larger beams bring more, but not necessarily useful, neutrons toward the sample and these extra neutrons have to be shielded. The collimator and a 1 m-long straight guide that follows are located in the core vessel insert of the SNS target (sections b and c, Fig. 1). They serve to facilitate the blockage of the direct line of sight from the neutron moderator as early as possible, while still passing thermal and cold neutrons to the sample location. Without them, either we would lose most of the less-collimated but still useful thermal and cold neutrons, or the core vessel insert would have to be opened up to allow those neutrons to pass through. In the latter case, the direct line of sight of the moderator would be shifted further downstream, making background shielding more difficult. In the absence of the collimator, the neutron guide would be at risk of thermal and radiation damage due to its close proximity to the moderator and target. Energy-deposition calculations and thermal analysis of the neutron guide show that, with the collimator, the temperature of the guide in the core vessel insert will be <303 K during normal beam operations (Murphy, 2003; Childs, 2003). In addition, since all optical components use non-borated float glass, the potential for radiation damage due to boron neutron absorption is greatly reduced.

The novel part of the beam optics is a curved multichannel beam bender, located in the primary beam shutter and the bulk shield insert of the target monolith (sections e and g, Fig. 1, and Fig. 2A). During routine instrument operation, the primary shutter remains in its open position. Its engagement is only needed for instrument maintenance. The insert in the primary shutter that hosts the multichannel beam bender is designed to return precisely to its aligned position each time the shutter is opened. The bender has a bending radius of 95 m and a total length of 3.3 m, which alters the direction of the neutron beam by 2°. Its side walls are made of 1 mm-thick float glass in order to allow close placement of the steel shielding pieces next to the beam. The bender has five curved inserts that divide the 40 × 40 mm neutron beam into six channels. These inserts are made of 0.55 mm-thick float glass. After the bender, sections of straight guides follow (sections i, j and k, Fig. 1), with gaps between them to accommodate three bandwidth choppers and a beam monitor.

The final choice of beam optical parameters was the result of extensive Monte Carlo simulations over a large range of possible configurations. With a larger bending radius or more channels, for example, the bender will perform better for transporting shorter-wavelength neutrons, which is desirable for extending the maximum Q range. However, a large bending radius means that the direct line of sight of the moderator is pushed further downstream, creating challenges for shielding the background. More channels mean that there will be more materials in the beam, reducing the neutron flux, especially for cold neutrons. At the collimation length of 4 m with a 20 × 20 mm sample at 14 m and a 40 × 40 mm source slit at 10 m, the flux gain by the EQ-SANS optics is at least a factor of 9 for $\lambda > 5$ Å neutrons. A more relevant comparison is with that of a straight guide alternative with the same $3.5\theta_c$ coatings, which is shown in Fig. 3. The ability of the EQ-SANS optics to transport $\lambda > 5$ Å neutrons is essentially the same as that of a straight guide. As already mentioned, using a straight guide in place of the bender requires that a T0 chopper be used.

With the collimator-guide–bender-guide optics, the last direct line of sight of the moderator is ∼8 m from the source. This leaves ∼5–6 m of shielding space between this last line-of-sight point and the sample at 14 m. The shielding materials

are composed of steel, heavy and light concrete, and thermal neutron absorbers (*e.g.* ^{10}B-containing materials). Detailed neutronic calculations were performed to verify all the shielding designs (Gallmeier, 2008).

The secondary shutter is a 1 m-long rotating drum (ScS, Fig. 1). It has four open and four closed positions. Currently, one of the open channels has a neutron guide installed. The other channels are reserved for future optical upgrades. The final collimation system consists of three slit wheels (S1–S3, Figs. 1 and 2D, with S1 installed at the time of writing) and a sample slit (Ss, Fig. 1). The sample slit is manually changeable. Each of the slit wheels has eight stepper-motor-driven positions. The slits in the slit wheels can be replaced during instrument maintenance. Currently, there are three circular (φ = 10, 15 and 20 mm) and three square (10 × 10, 15 × 15 and 20 × 20 mm) slits installed on each slit wheel. The other two slit positions are either fully open (40 × 40 mm) or fully closed.

After the collimation slits, there are six guard slits between S3 and Ss (Gs, Fig. 1). Their function is to reduce the instrument background by removing stray neutrons, such as those fast ones coming down the neutron guides, hitting the shielding behind the last line of sight of the moderator and moderated by the shielding materials. Finally, a removable W-shaped sapphire frame overlap mirror is designed between S2 and S3 for future upgrade. Each of the sapphire blades in the W is inclined at a 2° angle with respect to the beam axis. For all practical collimation setups on EQ-SANS, the frame overlap mirror will critically reflect neutrons of a wavelength $\lambda > 33$ Å out of the beam, but have no effect on those of $\lambda < 20$ Å. As will be discussed below, the chopper system on EQ-SANS is designed such that all higher-frame leakages occur at $\lambda > 38$ Å. Thus, the combination of the frame definition choppers and the frame overlap mirrors ensures a clean beam spectrum.

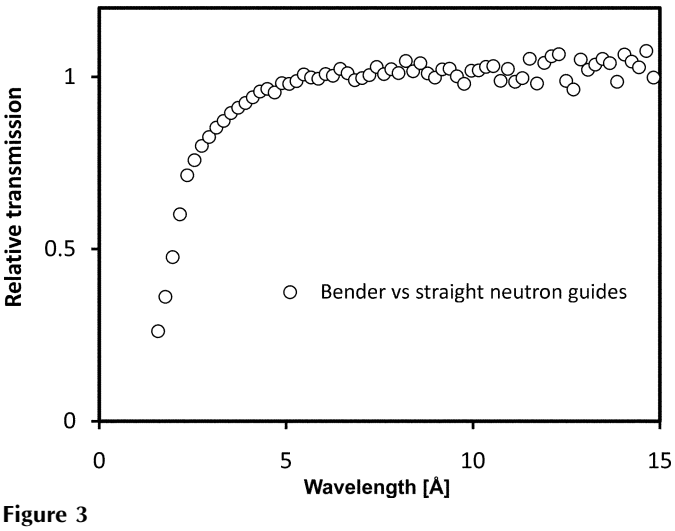

Figure 3
Simulated relative transmission of the EQ-SANS optics compared with the alternative of using straight guides. For the simulations, neutrons are counted at the sample position (14 m) behind a 20 × 20 mm sample slit. A 40 × 40 mm collimation slit is located at 10 m. For the alternative straight guides, the multichannel bender is replaced with a straight guide of the same cross section. A 0.5 m gap is introduced between the guides as a place holder for a T0 chopper. For both simulations, the divergence at the source is limited to ±1°, which is enough to illuminate the guides fully at the simulated collimation length.

Even with highly optimized neutron optics, there are additional ways to maximize the flux on the sample. One of these is to reduce the number of materials in the neutron flight path. Obviously, a good vacuum in the optics system is required. Another source of flux-attenuating material is the beam windows. Within the SNS target monolith, there are five windows along the EQ-SANS beam path, two at each end of the core vessel insert, two at the ends of the primary shutter and one at the beginning of the bulk shield insert (at positions b, d and f, Fig. 1). These windows are made of aluminium alloys (type 6061-T6, as specified in ASTM standards; Mayer, 2009). Since they mark vacuum boundaries and are within the SNS target monolith, they are made fairly thick for safety reasons. Except for the bulk shield insert window, which is 1 mm thick, the other four windows are 2 mm thick. Downstream from the bulk shield insert, the optics are enclosed in one vacuum chamber with only one additional beam window before the sample. This last beam window is made of single-crystal sapphire. The beam monitor, which is a low-efficiency ^{3}He detector supplied by Ordela (http://www.ordela.com), does have two aluminium windows but it does not interrupt the vacuum (M, Fig. 1). With this unified vacuum chamber, 14 potential windows around the three bandwidth-limiting choppers (four for each) and the beam monitor (two) are eliminated. Even with 6061-aluminium alloys, which have a high strength-to-neutron-absorption ratio, these 14 windows would have put ∼10–15 mm of materials in the beam, and the neutron absorption and scattering by them would have attenuated the beam by ∼10–15% for 5 Å neutrons. The attenuation increases for longer-wavelength neutrons.

Another area of neutron flux optimization is the off-centered beam optics. With its pinhole geometry, EQ-SANS views a rather limited area on the moderator surface. The size of the SNS Beamline 6 moderator surface is 100 × 140 mm. Neutron brightness is not uniform across the moderator: its lower upstream corner, which is closer to the SNS mercury target and the incoming proton beam, is more than twice as bright as its upper downstream corner (Iverson *et al.*, 2002; Ferguson, 2002). To take full advantage of this uneven brightness distribution, the EQ-SANS beam is shifted 20 mm downward and 20 mm upstream from the center line of the moderator surface. The corresponding flux gain is estimated at ∼20–30%. Together with the reduction in beam windows, these simple optimizations increase the beam flux at the sample by an estimated ∼30–40%, which is significant considering the challenges of increasing the power of a spallation source by the same amount.

4. Frame definition choppers

The EQ-SANS instrument has three bandwidth choppers designed for maximum operational flexibility. They are located 5.7, 7.8 and 9.5 m from the moderator (T1–T3, Fig. 1) (Zhao, 2003*b*) and were supplied by SKF (http://www.skf.com)

and Mirrotron (http://www.mirrotron.kfkipark.hu). The diameters of the chopper discs are 637 mm (Fig. 2B). The chopper motors have magnetic bearings that significantly reduce their maintenance needs. The boron coatings on the discs have a maximum transmission of 10^{-6} for 1 Å neutrons (http://www.mirrotron.kfkipark.hu). The T3 chopper consists of two single disc choppers separated by 10 mm. The two discs rotate at the same speed and in the same direction, but their relative phases can be changed. Therefore, T3 is considered as a double-disc chopper with a variable opening. The T1 and T2 choppers both have a single disc, although spaces have been reserved to allow them to be upgraded to double discs. The cut-outs on the discs have opening angles of 129.6° on T1, 180° on T2 and 230° on each of the T3 discs (Fig. 2B). To maintain upgrade flexibility, the chopper housings are designed such that the choppers can be translated up and down by 100 mm *via* remotely controlled motors. The plan for future upgrades is to install high-speed chopper discs such as that shown in Fig. 2B. The white dashed line in Fig. 2B indicates where the cut-out for the high-speed mode would be. Through the translocation of the choppers (Fig. 2C), EQ-SANS can be operated either in the current SANS mode or at higher chopper speeds in an inelastic mode. In the latter mode, the instrument is turned into a disc chopper spectrometer. While it will not be a highly optimized inelastic instrument, it offers a way of determining and separating inelastic contributions to small-angle scattering, which can be significant for soft materials.

4.1. 60 Hz operations

Because the EQ-SANS instrument has a variable moderator-to-detector distance, the bandwidth choppers need to allow variable neutron frames. The easiest way to achieve this is to use double discs for all three choppers. In practice, the same frame change can be accomplished in most cases through the phasing of the three choppers against each other. The cut-out openings on the T1 and T2 chopper discs allow a ∼4.2 Å wide neutron band at 60 Hz, which sets the upper limit for the width of a single frame. This bandwidth value corresponds to a detector location of ∼15.8 m (SDD = 1.8 m). The time diagram in Fig. 4 shows the operation of the choppers at the longer detector distance of 19 m. The opening of the T3 chopper is adjusted to the required frame width. To reduce higher-frame leakages, T1 is phase shifted and aligned with the trailing edge of the frame (λ = 6.9 Å), while T2 is aligned with the leading edge (λ = 3.5 Å). The first higher-frame leakage occurs at λ > 38 Å. This lower leakage threshold holds true for all frames and detector distances for 60 Hz operation.

4.2. Pulse rejection

To overcome the relatively narrow bandwidth of 3–4 Å at 60 Hz, it is possible to operate the EQ-SANS diffractometer in the so-called pulse-rejection mode. In this mode, the choppers are operated at 30 Hz and they reject every other pulse, while allowing twice the bandwidth from the non-rejected pulses to pass. The difficulty of such operations arises from the leakage from the rejected pulses. On the EQ-SANS instrument, the rejected pulses will leak through the choppers at λ < 20 Å for all pulse-rejection setups. For example, if the choppers are operated in the pulse-rejection mode with the same instrument setup as shown in Fig. 4, the neutron band would be twice as wide, λ = 3.5–10.4 Å. However, neutrons from the rejected pulses with wavelengths in the range λ ≃ 13.7–17.4 Å will pass through the choppers as well (Fig. 5). Unless a frame overlap mirror is in place to remove all these leaked neutrons, the collected data at the detector will be contaminated and not interpretable. The required frame overlap mirror will need to have a sharp wavelength cutoff very close to the desired wavelength band, which is not practical unless the neutrons are extremely well collimated. The mirror will also need to be tunable *in situ* in order not to limit the ability of the instrument to use longer wavelength neutrons from higher frames.

4.3. Frame skipping

As an alternative to the impractical pulse-rejection operation discussed above, a new mode of operation, frame skipping, is introduced on EQ-SANS. Similar to pulse rejection, the choppers are operated at 30 Hz. However, they are phased such that one frame, let us say frame 1, from the pulse at time zero passes through the choppers. At the same time, frame 3 from the previous pulse (at −16.6 ms) passes through as well (Fig. 6). These frames 1 and 3 arrive at the detector at different times of flight. The end result is that the total neutron band-

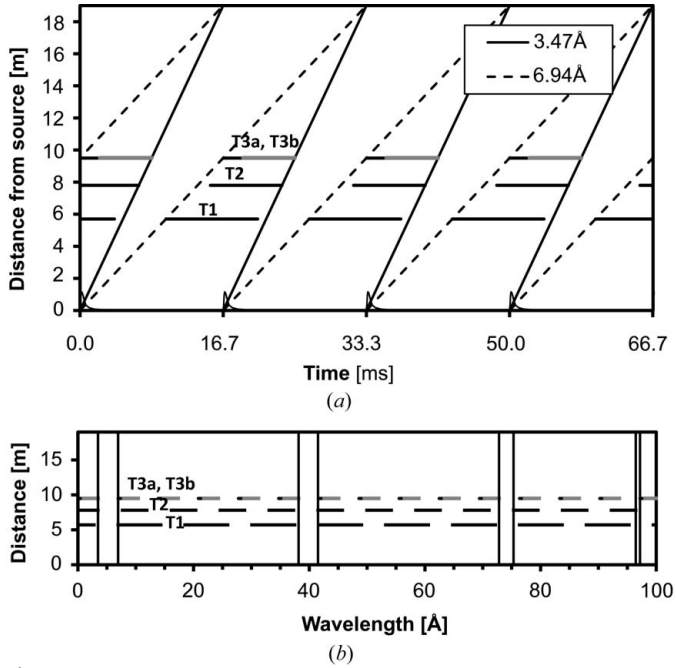

Figure 4
(*a*) Time diagram for 60 Hz operations for a source-to-detector distance of 19 m. The choppers are phased to the second frame (3.47–6.94 Å). The three choppers are labeled T1, T2, T3a and T3b. (*b*) The harmonics of neutron bands that can pass through the choppers. The higher frame harmonics, or leakages, will be eliminated from the neutron beam by a frame overlap mirror. For simplicity, the dimensions of the beam cross section and neutrons coming from the tail end of the source pulse are not considered in this diagram.

width is three times as wide as that at 60 Hz operation, equivalent to a 20 Hz SANS machine. No neutron pulse is rejected in the process and a frame in the middle is skipped over. The gap in Q space due to the missing frame 2 in the example is readily bridged by the two-dimensional detector on EQ-SANS. As an example setup, when the detector is at 19 m (SDD = 5 m) and with the starting wavelength for frame 1 set at 2 Å, the Q ranges covered by frames 1 and 3 are $Q_1 \simeq 0.003$–0.09 Å^{-1} and $Q_3 \simeq 0.007$–0.4 Å^{-1}, respectively, on the 1×1 m detector with a 50 mm thermal beam stop at the center of the detector.

For most SANS experiments, the difficulties often lie with obtaining good data at either the low-Q or high-Q end of the $I(Q)$ spectrum. At the low-Q end, extremely good neutron beam collimation is required for the pinhole type of SANS instruments, which drastically reduces the beam flux and the data counting rate. At the high-Q end, the difficulty is of a different origin. The scattering profile of most samples drops sharply with increased Q values. For systems that follow Porod's (1951) law for example, the scattering intensity decays as a function of Q^{-4} at higher Q values. Discounting the details of the spectroscopic distribution of the moderator and the wavelength dependency of small-angle scattering power, we can argue that, in the frame-skipping mode, frames 1 and 3 contribute more to either the high- or low-Q end of the data than the missing frame 2 would have done. Consequently, given the same source power per pulse, EQ-SANS operated in frame-skipping mode will be able to compete effectively with a similar instrument on a 20 Hz source.

It is noted that the frame-skipping operation can only be used when the distance of the detector from the moderator is no more than twice that of the last bandwidth chopper. Beyond that distance, frames 1 and 3 start to cross talk. Since the last chopper on EQ-SANS is at 9.5 m, frame skipping will be used only for detector locations of 19 m or less, namely for SDD $\leq$ 5 m. An incidental convenience from such a limitation is that, at these distances, the gravity drop for cold neutrons is insignificant, making it easier to design a beam stop that blocks the direct beam for all neutrons within a wide neutron band. For $\lambda = 10$ Å neutrons, for example, the drop between the sample and the detector is less than 1 mm at SDD $\leq$ 5 m. When the detector is at the end of the detector tank with SDD = 10 m, the same $\lambda = 10$ Å neutrons would have dropped more than 3 mm by the time they reach the detector after they have been scattered by the sample.

The feasibility and validity of frame skipping are demonstrated by the integrated scattering intensity of a vanadium sample, shown in Fig. 7. Since the neutron scattering cross section of vanadium is predominately incoherent, its integrated scattering data over the whole detector should be close to the neutron beam spectrum at the detector location. It is evident from the comparison of the vanadium data with the measured neutron flux at the sample location that the vanadium data are composed of two separate frames, with a frame in the middle being skipped.

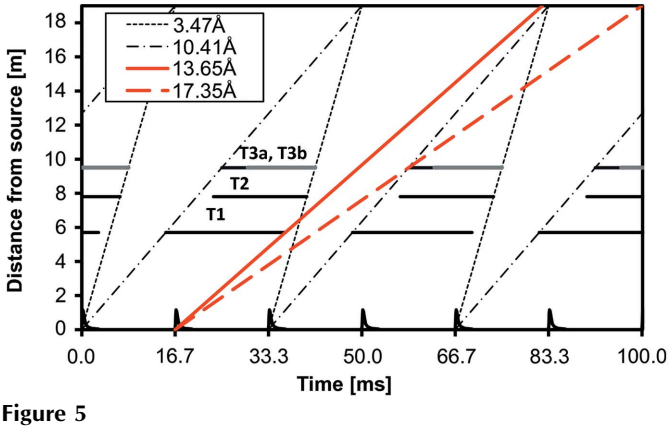

Figure 5
Time diagram for the 30 Hz pulse-rejection operation. The instrument setup is the same as that in Fig. 4. Higher frames from even-numbered pulses are effectively blocked by the choppers up to $\lambda = 65$ Å. However, neutrons in the range $\lambda = 13.65$–17.35 Å (thicker solid and dashed lines) from odd-numbered pulses will leak through, contaminating the beam. Delaying the opening of the T1 chopper improves the situation somewhat but will not eliminate the leakage.

5. Sample environment

The standard sample environment on the EQ-SANS instrument is an automated sample changer. For liquid samples,

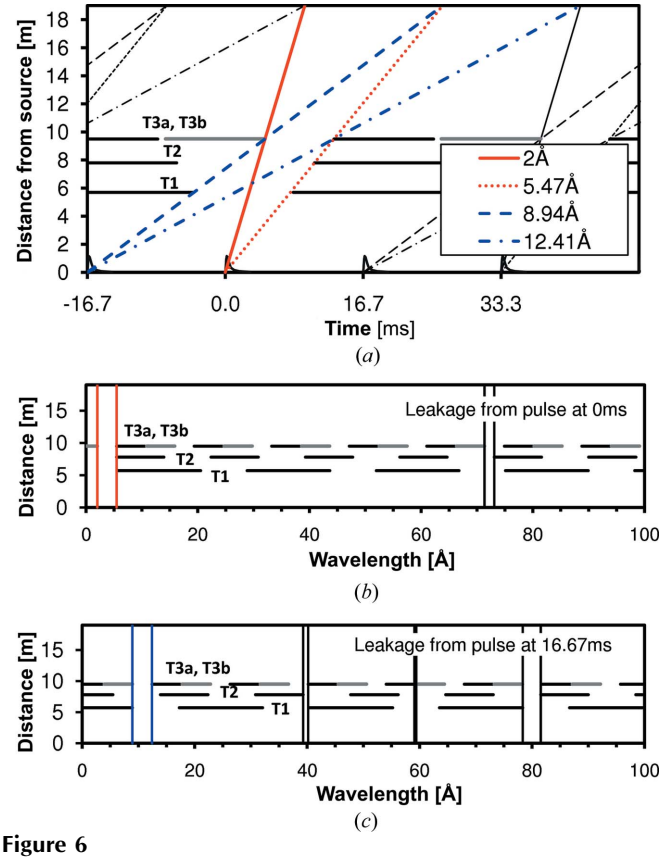

Figure 6
(*a*) Time diagram for the frame-skipping operation at 30 Hz with SDD = 19 m. Frames 1 from even-numbered pulses (at 0, 33.33 ms *etc.*) are allowed to pass through the choppers. At the same time, frames 3 from odd-numbered pulses (at −16.67, 16.67 ms *etc.*) are allowed to pass through as well. On the detector, these two frames do not overlap and can be treated separately. (*b*), (*c*) Neutron leakages through the choppers from even- and odd-numbered pulses, respectively.

rectangular or banjo-type optical cells with a thickness of 1–5 mm and a cross section of up to 20 × 20 mm can be mounted in the sample holder. Larger samples are possible with customized sample holders. The sample changer is designed to be temperature controlled between 253 and 353 K. It is located within a sample environment tank, which serves as a radiation shield and offers a humidity-controlled space around the sample. To be able to accommodate magnetic equipment, there is no significant quantity of magnetic material within a 2 m radius of the sample location. The sample environment tank, the front section of the detector tank (see next section) and the end sections of the collimation optics are all made of stainless steels.

6. Detector layout

The EQ-SANS instrument employs ^{3}He tubes for its low-angle detector (Fig. 2E), supplied by GE (http://www.gepower.com). They have an active length of 1041 mm and a diameter of 8 mm. Along the tube, the detector is electronically divided into 256 pixels of about 4.3 mm; the pixel size varies slightly with different electrical and electronic setups and needs to be calibrated when the setup changes. The physical resolution of the detector along the tube is determined by the applied high voltage. The EQ-SANS detector currently operates at ∼1625 V. The full width at half-maximum (FWHM) resolution of the detector tube at this voltage is ∼7 mm. The gas pressure in the tube is 22.1 bar, ∼20 bar of which is ^{3}He (1 bar = 100 000 Pa). To increase the counting efficiency of the whole detector, the tubes are arranged in two planes. Within each plane, the tubes are separated by 11 mm center to center. The two planes are 8.2 mm apart and the tubes between the planes are offset laterally by 5.5 mm. This arrangement is found to be a good compromise between ease of detector construction and achievement of a deep and uniform ^{3}He gas distribution across the detector. Fig. 8 shows the gas-depth distribution in the front view of the detector. Any closer tube arrangements will not significantly improve the distribution, while if the tubes are too far apart, neutrons with large scattering angles will see gaps between the tubes through both planes. In the front view, the average depth–pressure product of the ^{3}He gas is ∼18 cm bar, giving a neutron absorption efficiency of ∼92% for thermal neutrons (λ = 1.8 Å). The rate limit of each tube is of the order of several tens of kHz, bringing the total counting rate of the detector well over the MHz hurdle. In addition, the smaller tube diameter significantly reduces parallax at higher scattering angles. The detector has a total area of 1 × 1.4 m (currently 1 × 1 m is installed) and is located in an evacuated scattering tank. The two planes of tubes are arranged on an arc of radius 5 m centered towards the sample position. Using 8 mm ^{3}He tubes greatly increases maintenance flexibility. The detector can be operated with a few non-functioning tubes (see Fig. 9) and these defective tubes can be replaced in between experiments. To reach even higher Q values in the future, upgrade space has been reserved for installing a high-angle detector bank to cover scattering angles of 30–150°. These high-angle detectors will allow the instrument to study simultaneously low-angle scattering and high-angle diffraction on such phenomena as nucleation and crystallization.

The scattering tank sits on rails movable by 2 m along the beamline. This movement is designed to facilitate the usage of large sample environment equipment such as magnets. The tank has a double-sided wall with 200 mm of light concrete between the walls, and a 5 mm-thick layer of sintered boron carbide lines the inside of the tank. The concrete serves to moderate the fast neutrons that hit the tank, while the boron carbide absorbs the slowed-down neutrons after they enter the tank, thus reducing the background level on the detector. When the SNS source is off, the electronic background on the whole detector is around 1–2 counts s^{-1}. When the SNS is

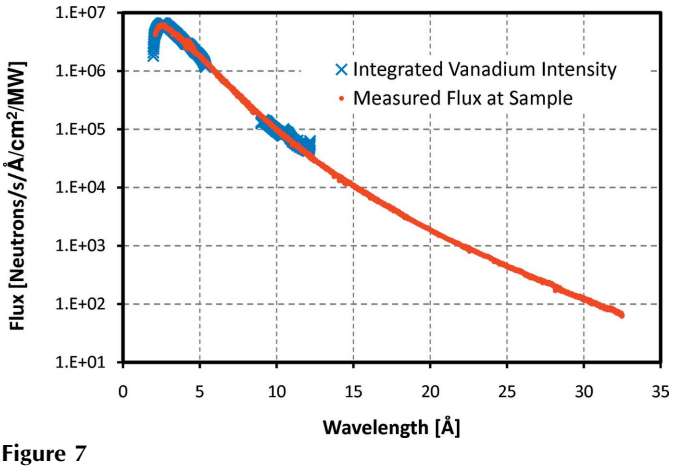

Figure 7
Integrated total scattering intensity over the whole detector from a vanadium sample, compared with the measured neutron flux at the sample location. The flux was measured directly on the detector 10 m away from the sample and with pinholes of various diameters (1–10 mm) at the sample location. The data are corrected for detector efficiency (see §6) and normalized to 1 MW of SNS source power. The collimation slit used (S1 in Fig. 1, collimation length 4 m) is 2 × 2 cm in size. The vanadium data are scaled to correspond to the measured flux. They are measured in frame-skipping mode at a detector distance of 19 m (SDD = 5 m) and a starting neutron wavelength of 2 Å. For clarity, fall offs at the ends of each frame due to the opening and closing of the bandwidth choppers (the edges of the chopper cut-outs sweeping through the neutron beam) have been trimmed off.

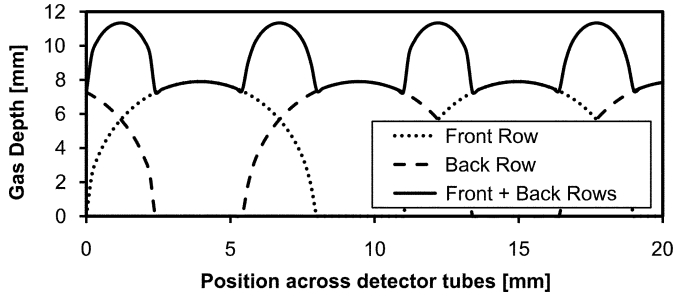

Figure 8
Front view of the ^{3}He gas depth across the tubes in the detector plane. The decrease in gas-depth homogeneity at larger scattering angles is not significant, except at the edges of the detector when the detector is less than 2 m from the sample. Even at SDD < 2 m, because the EQ-SANS detector tubes are arranged on an arc of 5 m radius, the gas-depth distribution across the detector plane is still very good.

running at 650 kW, which is about half of its design power, the total background on the detector is about 8–9 counts s^{-1} with the secondary shutter (ScS, Fig. 1) closed and the primary shutter either open or closed.

7. Instrument resolution

From the definition of neutron momentum transfer, $Q = (4\pi/\lambda)\sin\theta$, the Q resolution is readily written as (Bevington, 1969; Zhao, 2000*a*)

$$(\delta Q/Q)^2 = (\delta\lambda/\lambda)^2 + \cot^2\theta(\delta\theta)^2. \quad (1)$$

The uncertainty in the scattering angle 2θ is mainly caused by the finite dimensions of the collimation slit (source slit), the sample and the detector pixels. For the wavelength spread, since a neutron's TOF (t, in seconds) is related to its wavelength by

$$\lambda = th/(m_N L) = 3956t/L, \quad (2)$$

where the quantities h, m_N, λ and L are the same as those defined in §1, we have

$$\delta\lambda/\lambda = \delta t/t = (3956/L)(\delta t/\lambda). \quad (3)$$

Therefore, in the one-dimensional approximation and for small scattering angles, the Q resolution can be expressed as (Zhao, 2000*a*)

$$(\delta Q/Q)^2 = (\delta t/t)^2 + \tfrac{1}{4}\cot^2\theta[(d_1/L_1)^2 + (d_2/L_1 + d_2/L_2)^2 + (d_3/L_2)^2], \quad (4)$$

where d_1, d_2 and d_3 are the sizes of the source slit, the sample and the detector pixels, respectively, L_1 is the source-slit-to-sample distance and L_2 is the sample-to-detector distance. The factor of $\frac{1}{4}$ arises from the fact that θ is half the scattering angle. On EQ-SANS, the uncertainty in a neutron's TOF, δt, is primarily determined by the pulse width of the moderator. TOF spreading by the neutron transporting optics, and the time resolution of the detector and the counting electronics, are minimal and can be neglected. For the coupled supercritical hydrogen moderator that EQ-SANS views, the FWHM of the source pulse is about $\delta t = 20$ µs for 1 Å neutrons (Iverson *et al.*, 2002). At longer wavelengths, the FWHM δt scales roughly linearly with wavelength up to $\lambda \simeq 15$ Å. Therefore, for the purpose of the current discussion, we have $\delta t/\lambda = 2 \times 10^{-5}$ s Å^{-1}. For comparison, the detector TOF uncertainty, limited by the 8 mm diameter of the ^{3}He detector tubes (see §6), is about one order of magnitude less. Given the total instrument length of L = 15–24 m, the FWHM wavelength resolution of EQ-SANS is then $\delta\lambda/\lambda \simeq 0.33$–$0.53\%$. It is noted that these resolution discussions are based on Gaussian-like distributions. On reactor-based SANS instruments, the velocity selectors produce a wavelength distribution similar to a Gaussian. However, the pulses from the SNS moderator have long time tails and their distributions are not symmetric. Nonetheless, the $\delta\lambda/\lambda$ on EQ-SANS is about one order of magnitude better than that of a velocity selector, which is typically about 5–30%.

8. Data handling

The scattering data from EQ-SANS are saved as neutron events. Each event stores the location of the detected neutron on the detector and its time of flight. The events are also associated with the source pulse from which the neutron originated (Riedel, 2007). For most SANS experiments, the three-dimensional data (detector x and y, and TOF) are reduced to a one-dimensional intensity I *versus* Q. The data reduction can be performed in different ways. The common approach at the SNS is first to histogram the data into multiple TOF slices. Each slice, or histogram, is then azimuthally integrated in the same way as that on a steady-state source-

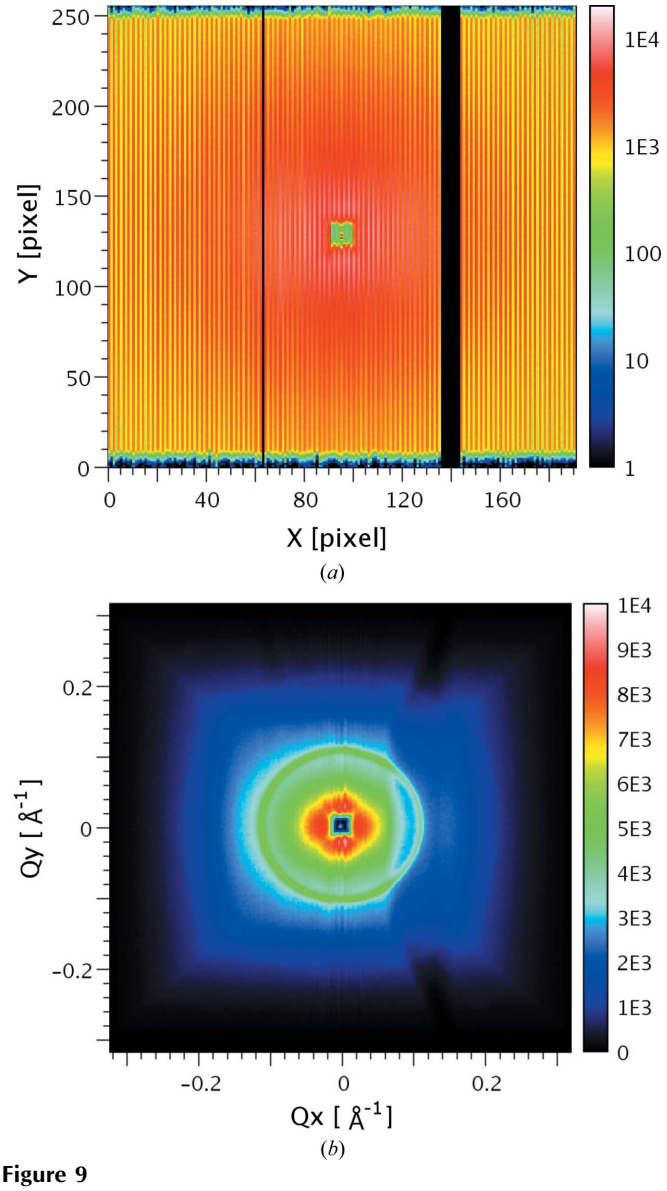

Figure 9
(*a*) Raw detector image of a silver behenate sample taken at 60 Hz operation, SDD = 3.9 m and a wavelength band of λ = 3–6.7 Å. The data were collected for 107 min and binned along the TOF axis. The plot is on a logarithmic color scale. Light and dark stripes correspond to detector tubes in the front and back rows of the detector, respectively. Nine detector tubes (at x = 63 and 136–143) were not functioning during this experiment. (*b*) The same data, binned along neutron momentum transfer axes Q_x and Q_y and plotted on a linear color scale.

based SANS instrument. Alternatively, the three-dimensional data can be reduced to $I(Q)$ directly, which is currently implemented on EQ-SANS. Each detected neutron is assigned to its corresponding Q bin according to its TOF and location on the detector, weighted by the detector solid angle that corresponds to this Q bin, in much the same way that azimuthal integrations do. One aspect of the $I(Q)$ integration that needs some attention is the gravity drop for cold neutrons during their flight from the sample to the detector. For experimental setups with SDD $\leq$ 5 m, such drops are not significant and ignoring them will only minimally degrade the Q resolution. However, if the detector is at the back of the scattering tank (SDD = 10 m), the drop for 10–15 Å neutrons becomes comparable to the pixel size on the low-angle detector. In these cases, the gravity drop is added back to the vertical position of the detected neutron before the neutron event is converted to Q-space values.

Systematic errors in the scattering data that originate from instrumental imperfections are corrected before those data are further analyzed. The dark current, which is measured during normal SNS operation but with the EQ-SANS beam shutter closed, is subtracted from the data. This dark current includes the electronic noise in the detector and the ambient background around the instrument. It is an additive effect and the subtraction is performed on data that are normalized by their measuring time. Subtraction of an empty beam measurement may also be needed, which aims to correct for the background created by the transmitted direct beam scattered off the beam stop. Other types of corrections are mostly multiplicative in their effects on the data. These include uneven source spectroscopic distribution and detector efficiency. The fact that scattered neutrons with different wavelengths cover different Q ranges also affects $I(Q)$ if its integration over different TOFs is simply carried out by summation. These multiplicative effects can be corrected individually or collectively through division of the measured spectrum of isotropic scattering.

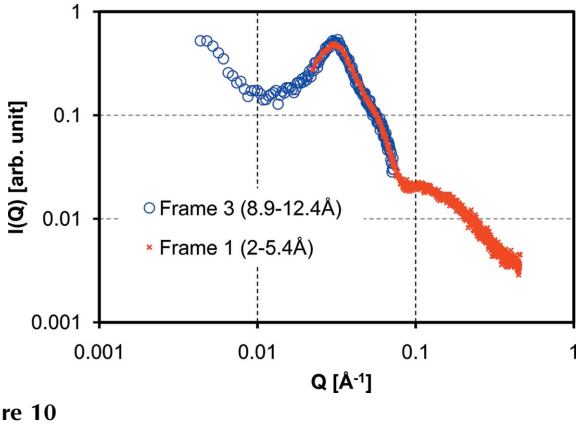

Figure 10
Reduced $I(Q)$ data from a dendrimer sample (Liu, 2010), measured with frame skipping and a sample-to-detector distance of 5 m. The sample is 10 × 10 mm in cross section and 1 mm thick. The collimation slit used (S1, Fig. 1) was 15 × 15 mm in size. The data collection time was 10 min. The statistical error bars are smaller than the size of the symbols. The data have been reduced for each frame separately to illustrate the Q range covered by each frame.

Other types of data treatment include the subtraction of the scattering contribution from the cell that holds the sample, or from buffer solutions in the case of liquid samples. Before these subtractions, the data are normalized by the source flux, which is measured at the beam monitor (M, Fig. 1). The proton current from the SNS accelerator can also be used to normalize the data. For a two-component scattering system such as a sample and a sample cell, it is readily shown that, in the absence of multiple scattering within each of the components, the scattering intensity I can be expressed as

$$I_{1+2}/T_{1+2} = I_1/T_1 + I_2/T_2, \tag{5}$$

where T is the transmission and the subscripts denote components 1, 2, or 1 and 2 together ($T_{1+2} = T_1T_2$). Therefore, if a nanoparticle sample is measured in a buffer solution, the scattering from the nanoparticles is readily obtained from two separate measurements of I_{s+b} and I_b:

$$I_s/T_s = I_{s+b}/T_{s+b} - I_b/T_b, \tag{6}$$

where the subscripts s and b denote the nanoparticle sample and the buffer, respectively. T_s is commonly omitted from the equation. On EQ-SANS, the transmissions are measured through a small pinhole in the middle of the beam stop (~0.1–0.3 mm). There are no neutron-attenuating materials along the path of the pinhole. Therefore, the TOF spectrum of the measured transmission can be used to approximate the spectroscopic distribution of the source. The scattering data from the sample can be put on an absolute scale by comparing them with the scattering data of a known scatterer. The absolute scale is the total scattering cross section per unit volume of the sample, usually in units of cm^{-1}.

The SNS data structure allows slicing of the experimental data after the experiments have been conducted. Essentially, each detected neutron event carries an absolute time stamp saved as the neutron's TOF and a reference time for the source pulse. Using these time stamps, time-dependent experimental phenomena can be readily studied. It is noted that the SNS source power level may not stay constant during an experiment. When performing time slicing, the sliced data need to be normalized to the source flux. However, the beamline monitor (M, Fig. 1) currently saves its data in TOF histograms and cannot be used for this purpose. The proton charge per pulse of the SNS accelerator is used in this case. Error handling on EQ-SANS data follows standard procedures, as described by Bevington (1969).

9. Initial experimental data

Fig. 9 shows two-dimensional scattering data from a 9.5 × 9.5 mm silver behenate (Gilles *et al.*, 1998) sample, which is used for Q calibration on EQ-SANS. The data were collected at a sample-to-detector distance of 3.9 m at 60 Hz and a wavelength band of λ = 3–6.7 Å. From the time-integrated raw data, the tubes in the front and back detector planes are visible.

Fig. 10 shows the reduced $I(Q)$ data from a dendrimer sample (Liu, 2010). The data were collected at a sample-to-

detector distance of 5 m using frame skipping with a starting wavelength of 2 Å. The total Q range covered by this single experimental setting is $Q \simeq 0.003$–0.4 Å^{-1}. The total data collection time of the actual experiment was 25 h, but the data shown in Fig. 10 are from the first 10 min only, extracted using the time stamps from the neutron events. During this experiment, the SNS source was run at a power level of <500 kW. Clearly, the instrument performs exceedingly well in terms of both its covered Q range and its counting statistics.

10. Summary

The EQ-SANS diffractometer has achieved its design goals of having high-intensity wide Q coverage and good wavelength resolution. The unique frame-skipping operation enables the machine to have a wide dynamic Q range equivalent to that of a 20 Hz SANS machine. The instrument is ready to serve the user community and become scientifically productive over the foreseeable future.

The construction of a neutron scattering instrument is a resource-demanding undertaking. The authors are extremely grateful to all the engineering, installation and project management support that the EQ-SANS instrument received throughout its construction. R. Summer, K. Chipley and D. Conner provided engineering support for the instrument. L. Funk and J. Barncord assembled, tested and calibrated all the detector tubes and ensured their proper functioning. J. Stockton and R. Lee provided support on the bandwidth choppers. J. Wenzel built the sample changer for the instrument. K. Crawford and B. Thibadeau managed the construction project that tracks all the resources and its progress. Without these efforts, the EQ-SANS instrument would not have become a reality. The authors are also grateful to all the encouraging colleagues without whom this work would not have been fun and successful. This manuscript has been authored by UT-Battelle, LLC, under contract No. DE-AC05-00OR22725 with the US Department of Energy. The United States Government retains, and the publisher, by accepting the article for publication, acknowledges that the United States Government retains, a non-exclusive paid-up irrevocable world-wide license to publish or reproduce the published form of this manuscript, or allow others to do so, for United States Government purposes.

References

Bevington, P. R. (1969). *Data Reduction and Error Analysis for the Physical Sciences*. New York: McGraw–Hill.

Childs, K. W. (2003). *Thermal Analysis of the 06td SANS Diffractometer Core Vessel Insert and Guide*. SNS Document SNS-107080600-DA0005-R00. Oak Ridge, Tennessee, USA.

Crawford, R. K. & Carpenter, J. M. (1988). *J. Appl. Cryst.* **21**, 589–601.

Crawford, R. K., Felcher, G. P., Kleb, R., Epperson, J. E. & Thiyagarajan, P. (1989). *Inst. Phys. Conf. Ser.* **97**, 257–262.

Dewhurst, C. D. (2008). *Meas. Sci. Technol.* **19**, 034007.

Ferguson, P. D. (2002). SNS internal communication and presentation to the Experimental Facility Advisory Committee meeting, April 3–5, 2002. Oak Ridge, Tennessee, USA.

Gallmeier, F. X. (2008). *EQSANS Beamline Shielding Calculations for the Final Instrument Configuration*. SNS Document SNS-107080700-DA0005-R01. Oak Ridge, Tennessee, USA.

Gilles, R., Keiderling, U. & Wiedenmann, A. (1998). *J. Appl. Cryst.* **31**, 957–959.

Glinka, C. J., Barker, J. G., Hammouda, B., Krueger, S., Moyer, J. J. & Orts, W. J. (1998). *J. Appl. Cryst.* **31**, 430–445.

Heenan, R. K., Penfold, J. & King, S. M. (1997). *J. Appl. Cryst.* **30**, 1140–1147.

Ibel, K. (1976). *J. Appl. Cryst.* **9**, 296–309.

Ishikawa, Y., Furusaka, M., Niimura, N., Arai, M. & Hasegawa, K. (1986). *J. Appl. Cryst.* **19**, 229–242.

Iverson, E. B., Ferguson, P. D., Gallmeier, F. X. & Popova, I. I. (2002). *Neutronics Calculations for Scattering Instrument Design: SCT Configuration*. SNS Document SNS-110040300-DA0001-R00. Oak Ridge, Tennessee, USA.

Koehler, W. C. (1986). *Physica B+C*, **137**, 320–329.

Liu, D., Chen, W.-R., Hong, K., Gao, C. Y., Melnichenko, Y., Littrell, K., Smith, G. & Zhao, J. K. (2010). Personal communication.

Mayer, V. A., Bailey, S. J., Baldini, N. C., Emery, S., Ermigiotti, J., Huffman, B. C., Morre, E., Olcese, E., Perters, K. A., Rosiak, J. L., Wright, J. & Furcola, N. (2009). Editors. *Annual Book of ASTM Standards*, Vol. 02.02, *Aluminium and Magnesium Alloys*. West Conshohocken: ASTM International.

Murphy, B. D. (2003). *Extended Energy-Deposition and Damage Calculations in Core-Vessel Inserts at the Spallation Neutron Source*. SNS Document SNS-107030600-DA0001-R01. Oak Ridge, Tennessee, USA.

Porod, G. (1951). *Kolloid. Z.* **124**, 83–103.

Riedel, R. (2007). *SNS Instrument Systems Data Acquisition File Formats Technical Reference Manual*. SNS Document SNS-107030200-TD005-R04. Oak Ridge, Tennessee, USA.

Seeger, P. A. & Hjelm, R. P. (1991). *J. Appl. Cryst.* **24**, 467–478.

Serdyuk, I. N. (1995). *Physica B*, **213**, 892–894.

Zhao, J. K. (2000*a*). *Conceptual Design and Performance Analysis of the Extended Q-range High-Intensity High-Precision Small-Angle Diffractometer for SNS*. SNS Document 107080100-TD0001-R00. Oak Ridge, Tennessee, USA.

Zhao, J. K. (2000*b*). ICANS-XV, Tsukuba, Japan, 6–9 November 2000, KEK Proceedings 2000–22, pp. 466–470.

Zhao, J. K. (2003*a*). *Optical Components for the Extended Q-Range Small-Angle Diffractometer at the SNS*. SNS Document SNS-107080600-TD001-R00. Oak Ridge, Tennessee, USA.

Zhao, J. K. (2003*b*). *Chopper Design and Operation for the EQ-SANS*. SNS Document SNS-107080400-TD0001-R00. Oak Ridge, Tennessee, USA.